Robotics and Computer–Integrated Manufacturing 74 (2022) 102282

Contents lists available at ScienceDirect

Robotics and Computer-Integrated Manufacturing

journal homepage: www.elsevier.com/locate/rcm

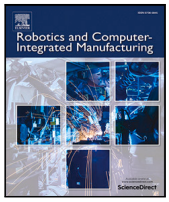

Full length article

Residual vibration suppression in uncertain systems: A robust structural modification approach to trajectory planning

Paolo Boscariol *, Dario Richiedei, Iacopo Tamellin

Dipartimento di Tecnica e Gestione dei sistemi Industriali - DTG Università degli Studi di Padova, Stradella S. Nicola 3, 36100 Vicenza, Italy

ARTICLE INFO

Keywords:
Uncertain flexible systems
Underactuated systems
Residual vibration suppression
Structural modification
Input shaping

ABSTRACT

In this paper a novel method to improve the residual vibration suppression in underactuated uncertain flexible systems through motion planning is proposed. The proposed technique relies on the concurrent use of input shaping and on the alteration of the mechanical properties of the system, which enables the enhancement of the robustness to uncertain parameters. Robustness is formulated through the parametric sensitivities of the natural frequencies that provide an analytical and non-probabilistic tool, which is embedded in the eigenstructure assignment algorithm developed in this work. The effectiveness of the proposed method is assessed through a benchmark testbed composed by a triple pendulum attached to a delta robot, that should execute rest-to-rest, residual vibration-free motion. Hence, residual vibrations of the pendulum are used to measure the accuracy and the sensitivity of the proposed combined shaper-IDSM approach. Both the numerical and experimental results confirm the advantages of the proposed technique for the suppression of the residual vibrations in uncertain systems over traditional techniques. In particular, robustness of the dominant tuning frequency is increased with respect to variations of the tip-end mass of the pendulum, representing a varying payload transferred by a robotic system.

1. Introduction

1.1. State of the art and motivations

Vibration suppression is still one of the most prominent challenges in the design and operation of automatic machines and robots. The rapid motions required to reduce the execution times result often, and especially for lightweight and high dynamics machines, in severe motion-induced vibrations that can last even after motion completion, severely affecting the effectiveness and precision of the machine.

The vast literature that has brought the development of methods to reduce motion-induced vibrations can be classified into ‘software’ approaches and ‘hardware’ approaches. A ‘software’ solution is applied whenever vibration reduction is obtained through a specific control action. For example, in [1] robust adaptive control is exploited to suppress vibrations in offshore ocean thermal energy conversion systems. Similarly, in [2] an adaptive fault-tolerant controller is designed to absorb vibrations in a flexible Timoshenko arm with backlash-like hysteresis. Alternatively, vibration suppression can be enforced, totally or partially, by carefully tuning the reference input [3–5] to the control, rather than acting on the control itself. In this case vibration suppression is enforced at motion design level, usually on the basis of some knowledge of the system in which vibrations are to be damped.

Hardware solutions, on the other hand, require some sort of physical alteration to the system under investigation. This alteration can be defined at system design level, by carefully tuning the system response according to some specifications, or at user level by providing some modifications or by introducing some additional elements that can absorb vibrations.

This very rough distinction provides a dichotomous classification of an extremely large corpus of methods and applications: in particular control-based methods are so commonly applied in literature that it is safe to state that every single control architecture has been applied to a vibration suppression problem at least once. Literature reviews such as [6–10] can guide the reader through a wide array of methods and solutions. The classifications of motion design-based methods is maybe more straightforward, since a first distinction can be made into model-based and model-free approaches. Model-free approaches generally work by enforcing the smoothness of the motion profile [11], under the assumption that a smoother motion profile provides minimal excitation of the oscillatory behavior [12,13].

In model-based methods partial or full information on the dynamic properties of the system to be moved in a vibration-free manner is exploited for the motion design problem — either using direct methods, such as [14–16], or indirect methods, such as [17,18]. As the name

* Corresponding author.
E-mail address: paolo.boscariol@unipd.it (P. Boscariol).

https://doi.org/10.1016/j.rcim.2021.102282
Received 29 April 2021; Received in revised form 9 September 2021; Accepted 15 October 2021
Available online 9 November 2021

suggests, direct methods are focused on the explicit design of a motion profile (or a trajectory) that enforces the required properties, while in indirect methods the motion design problem is cast – and solved – as a variational problem [19,20]. Both methods have their pros and cons and their field of applications, however indirect methods are favored for their accuracy, but are often plagued by a small radius of convergence and the applicability to problems limited in size [21].

The problem of residual vibration reduction can be tackled, however, also by using a very simple solution, which applies to all systems whose dynamics can be effectively represented by a linear model: input shaping [22]. Input shapers, which are convolution filters, can be applied to an arbitrary motion profile, achieving, at least theoretically, zero residual vibrations. Their popularity is due to their very simple tuning: the design of an input shaper requires just the knowledge of the frequency and damping factor of the oscillation that is to be canceled. Whenever two or more modes are to be dealt with, two or more input shapers can be cascaded. This technique has proved, over the years, to be rather effective, at least within its main limitations, the first one being the delay introduced by the shaper, which is inversely proportional to the frequency to be canceled: hence shapers are generally unsuited to fast motion profiles [23]. The second limitation is their capability of handling uncertainties in the determination of the oscillating mode properties, which is rather poor in standard methods, as in the popular Zero-Vibration (ZV shaper). The enhancement of the robustness properties of ZV shapers has lead to the development of robust shapers, the most popular one being the ZVD and the EI shapers [24], which exhibit a noticeable better performance for uncertain systems, but at the cost of even higher delays.

The popularity of robust solution in input shaping is the response to a common problem, i.e. the precise determination of the modal properties of the system to be moved with limited vibrations. This occurrence is rather common in many practical situations, as an unmodeled or unmeasured significant alteration of even the main oscillating frequency can happen, for example, by altering the payload that is transferred, in the case of an industrial robot, or simply by changing the length of the rope in a cable-suspended load system, just to cite two common occurrences.

The oscillatory behavior of a system is related to its eigenstructure, which is in turn determined by the eigenvalues (natural frequencies and damping ratios) and eigenvectors (mode shapes). The former define the settling time and speed of response, while the latter define the spatial shape of the vibration. Allowing to alter the eigenstructure of the system opens a new set of possibilities, assuming that a 'better' eigenstructure can lead to 'improved' performances. This is the key idea that has lead to the development of Eigenstructure Assignment (EA) methods. EA has been a core research area in vibration control in the last decades [25]. Active approaches, that employ the energy of actuators fed by the information gathered by sensors, have been widely studied and several techniques based on the system model or on the measured receptances have been proposed (see e.g. [26–30] and the references therein). Despite the generally high performances of these techniques two main limitations arise: first, costs. Secondly and mainly, the controlled system may become unstable and such problem is exacerbated in the presence of uncertainties. In the light of these limitations, passive techniques, based on the modification of the physical system (e.g. through masses, springs or dampers) have been proposed: they are usually referred to as an Inverse Dynamic Structural Modification (IDSM) methods. Indeed, IDSM is particularly attractive due to the inherent stability of the modified system, which can be preserved by enforcing the symmetry and positive-definiteness of the structural modifications. Several approaches to the IDSM have been developed to perform the assignment of: natural frequencies [31–33], mode shapes [34,35], vibration nodes [36], optimal design of dampers [37] or antiresonances [38,39].

The main limitation of the existing IDSM techniques is that robustness is usually not addressed: in particular the effect of parametric variations on the system natural frequencies is in most cases neglected. Clearly, the attainment of a "robust design" for the everyday functionality of mechanical flexible systems is particularly attractive [40]. However, up to now robust design has been mainly considered to achieve strength of materials and components by trading between over-sizing and reliability [41].

In IDSM some ad-hoc solutions have been proposed to tackle some specific problems, which testify the many possible applications of such technique. For example, in [42,43] the robust design of brakes with respect to self-excited vibrations is solved by maximizing the spectral gap between consecutive natural frequencies. A probabilistic approach for the robust design of flexible rotor-bearing systems is proposed in [44]: in this particular problem, natural frequencies are to be assigned as far as possible from the rotational speeds of the machine. In [45] a robust design to tackle self-excited vibrations due to frictional force in screw jacks is developed using the analytic expression of the natural frequencies of a two d.o.f. system. Robustness against uncertain excitation frequency is considered in the design of tuned mass dampers for vibration absorption in [46,47]. In that case, the goal is to ensure a low gain in the transfer function from the excitation force to the response of the main system in such a way that a robust vibration absorption is achieved.

Differently, in this work it is wanted to achieve robustness of the assigned natural frequencies with respect to parameter changes. A non-probabilistic robustness requirement, particularly useful when probabilistic distribution for the parameter variations are not available, is adopted through the assignment of the system sensitivities.

1.2. Contributions of this paper

In the light of the limitations of the existing literature in handling system uncertainties for Inverse Dynamic Structural Modification and due to the industrial ever-growing adoption of lightweight and thus vibration-prone systems, this paper proposes a novel approach to the vibration reduction for the trajectory planning for underactuated and uncertain dynamic systems.

In this work an alternative approach is proposed, which is to be referred to as a 'mixed' solution, being based on the concurrent application of 'software' shaping technique and on the 'hardware' modification of the physical properties of the system to be moved, with the explicit intent of enhancing its parametric robustness, i.e. to reduce the effects of disturbances or of uncertainties on is dynamic properties.

The method is based on the concurrent redesign of the motion profile, using input shaping, and of the mechanical structure of the system to be moved, using the robust assignment of one or more natural frequencies with respect to one or more uncertain parameters. The method is of general formulation, thus it overcomes the limitation of the state-of-the-art ad-hoc provided solutions. The IDSM is solved exploiting a constrained least-square problem that embeds a non-probabilistic robustness requirement and partially assigns the system mode shapes. The solution method ensures technical and economical feasibility of the achieved structural modifications. The effectiveness of the proposed method is assessed through both numerical simulations and experimental tests on a triple pendulum excited by the motion of a parallel robot: the signals of interest are recorded through a motion capture system which uses four high-speed cameras.

2. Residual vibration and formulation of the inverse dynamic structural modification

2.1. Suppression of residual vibration

It is well known that the execution of high-dynamic motion by underactuated flexible systems can lead to unwanted large steady-state vibration if the motion profile is not carefully planned. As mentioned before, an effective and widely employed technique to suppress the

residual steady-state vibrations is the input shaping technique which relies on a redefinition of the reference trajectory by convolving it with a finite sequence of impulses applied at prescribed time intervals [22]. The shaped trajectory $y^{r,s}$ is formed by performing one or more repetitions shifted in the time, and scaled in amplitude, of the unshaped trajectory $y^{r,u}$. Input shaping techniques are effective if the amplitude of the impulses and the time intervals between the impulses are correctly set according to the system natural frequency ω_n and damping ratio ξ. As such, the effectiveness in the elimination of the residual vibration is directly proportional to the accuracy of the adopted dynamic model [48]. In this work, two most commonly used input shapers will be considered: the ZV and the ZVD.

Let us consider, without loss of generality, a single DOF oscillatory system. The free response of the system after a sequence of n impulses, each one applied at time t_i and with amplitude A_i, can be analytically evaluated as [49]:

$$\begin{aligned} A_{out} &= \frac{\omega_n}{\sqrt{1-\xi^2}} e^{-\xi\omega_n t_n} \sqrt{\left(C\left(\omega_n,\xi\right)\right)^2 + \left(S\left(\omega_n,\xi\right)\right)^2} \\ &= \frac{\omega_n}{\sqrt{1-\xi^2}} V(\omega_n,\xi) \end{aligned} \tag{1}$$

where $V(\omega_n,\xi)$ is the Percentage Residual Vibration (PRV) and:

$$\begin{aligned} C\left(\omega_n,\xi\right) &= \sum_{i=1}^{n} A_i e^{\xi\omega_n t_i} \cos\left(\omega_n t_i \sqrt{1-\xi^2}\right) \\ S\left(\omega_n,\xi\right) &= \sum_{i=1}^{n} A_i e^{\xi\omega_n t_i} \sin\left(\omega_n t_i \sqrt{1-\xi^2}\right) \end{aligned} \tag{2}$$

Setting Eq. (1) to zero ensures that zero residual vibration is achieved by a proper sequence of pulses: as shown, for example in [50], this requires just two pulses for a single mode oscillating systems. The two pulses must have proper amplitudes A_1 and A_2, and must be timed properly with t_1 and t_2, with t_1 conventionally set to zero. The sequence of pulses can then be replaced by a convolution filter, which can be applied to an arbitrary reference signal $y^{r,u}(s)$, according to:

$$y^{r,s}(s) = \left(\frac{1}{1+K} + \frac{K}{1+K} e^{-s\frac{\tau_d}{2}}\right) y^{r,u}(s) \tag{3}$$

where s is the Laplace operator, $K = e^{-\frac{\xi\pi}{\sqrt{1-\xi^2}}}$ and τ_d is the damped vibration period. Intuitively, the ZV shaper places the second pulse half of the damped oscillation period after the first one and properly scales it with respect to the first pulse, with scaling factors equal to $K/(1+K)$ and $1/(1+K)$: they add up to 1 so that the amplitude of the unshaped signal is retained after the filtering.

The ZV shaper is effective and widely employed, however its main drawback is related to its limited robustness: its vibration canceling capabilities are severely affected by even modest model-plant mismatches. Indeed, if the actual natural frequency of the system deviates from the nominal one, the effectiveness of the ZV decreases since the canceling interference between sinusoidal waves is only partially obtained: hence residual vibrations can occur. The analysis of the sensitivity of the PRV with respect to the natural frequency of the system, i.e. $\partial V(\omega_n,\xi)/\partial\omega_n$, enables to investigate the robustness of the adopted shaper.

In the light of the non-negligible sensitivity of the ZV shaper the ZVD shaper has been later developed. The chief idea is to introduce an additional robustness constraints by setting equal to zero also the derivative of PRV curve in the neighborhood of the nominal frequency. To achieve this result the following constraint is introduced:

$$\frac{\partial V(\omega_n,\xi)}{\partial\omega_n} = 0 \tag{4}$$

The shaped reference signal is obtained as follows [50]:

$$y^{r,s}(s) = \left(\frac{1}{1+2K+K^2} + \frac{2K}{1+2K+K^2} e^{-s\frac{\tau_d}{2}} + \frac{K^2}{1+2K+K^2} e^{-s\tau_d}\right) y^{r,u}(s) \tag{5}$$

Hence, differently to the ZV, three impulses are needed to cancel a single-mode: the delays can be recognized in Eq. (5) as: $t_1 = 0$, $t_2 = \tau_d/2$, $t_3 = \tau_d$, while the amplitudes are the three coefficients that depend on K.

It is worth to notice that the delay introduced by the ZVD shaper ($t_s = \tau_d$) is double with respect to the one of the ZV shaper ($t_s = \tau_d/2$), i.e. to achieve higher robustness the ZVD shaper requires that either motion time is increased, or the unshaped motion profile duration is reduced (i.e. compensated), with an increase of velocities and acceleration peak values.

Shapers with enhanced robustness have been introduced considering higher order of derivative for Eq. (4) leading to the ZVDD, ZVDDD and so on [50]. However, each order of derivative requires the introduction of a further delay equal to $\tau_d/2$ which leads to an even higher increase of velocities and accelerations, or to a substantial increases of the motion time.

Input shapers have been developed to suppress the steady-state vibration arising from a single-mode, however, multiple modes can be tackled as well simply by placing several ZV or ZVD shapers in cascade, and by making sure that each of them is properly tuned to suppress the prescribed mode.

The ZV and the ZVD shapers can be considered a 'loosely' model-based strategy, since they do take into account only the essential property of the system, i.e. the natural frequency ω_n and damping factor ξ, but no specific information is required on the source of uncertainty, that can be either due to model-plant mismatches, parametric deviations, control inaccuracies, as well as caused by external disturbances. Conversely, a peculiar advantage of the variational approach proposed in [23] is its capability of directly considering the sensitivity of the residual oscillation with respect to the source of uncertainty, i.e. the deviation of one of the system parameters, by embedding it in the formulation of the system dynamics.

Let us define the uncertain parameter ϑ and let us consider the sensitivity of the PRV with respect to this parameter, i.e. $\partial V(\omega_n,\xi)/\partial\vartheta$. The latter can be rewritten into the more convenient form:

$$\frac{\partial V(\omega_n,\xi)}{\partial\vartheta} = \frac{\partial V(\omega_n,\xi)}{\partial\omega_n}\frac{\partial\omega_n}{\partial\vartheta} \tag{6}$$

Eq. (6) reveals that once the number of impulses is given, i.e. $\partial V(\omega_n,\xi)/\partial\omega_n$ is fixed, an effective approach for increasing the robustness of the PRV to parametric deviations is to minimize the sensitivity of the natural frequency with respect to the uncertain parameter, i.e. $\partial\omega_n/\partial\vartheta$. Such problem is non-trivial and the difficulties are exacerbated for underactuated multi-DOFs systems. In the light of this issue, a general framework to cope with this task is proposed in this paper.

2.2. Theoretical background on the eigenstructure of flexible systems

Let us consider an N-DOFs undamped vibrating system modeled through its symmetric and positive-definite mass and symmetric and positive-semidefinite stiffness matrices, respectively denoted $\mathbf{M} = \mathbf{M}^T > 0$ and $\mathbf{K} = \mathbf{K}^T \geq 0$.

The equations of motion of the system are expressed by the matrix form:

$$\mathbf{M}\ddot{\mathbf{q}}(t) + \mathbf{K}\mathbf{q}(t) = \mathbf{B}\mathbf{f}(t) \tag{7}$$

where $\mathbf{M}, \mathbf{K} \in \mathbb{R}^{N\times N}$. $\mathbf{B} \in \mathbb{R}^{N\times N_b}$ is the actuation matrix and $\mathbf{f} \in \mathbb{R}^{N_b}$ is the vector of the N_b external forces, while $\mathbf{q} \in \mathbb{R}^N$ is the vector of the N free coordinates of the system.

Eq. (7) is evaluated in the frequency domain (ω) and the free response of the system is obtained by solving the following eigenproblem:

$$\left(-\omega_{n,i}^2\mathbf{M} + \mathbf{K}\right)\mathbf{u}_i = \mathbf{0} \quad \text{with} \quad i = 1,\ldots,N \tag{8}$$

where $\omega_{n,i}$ is the ith natural frequency of the system and $\mathbf{u}_i$ is the related ith mode shape: together they constitute the eigenpair $(\omega_{n,i}, \mathbf{u}_i)$.

The system parameters are often affected by several sources of uncertainty, that might be caused by imperfections in the manufacturing process, aging, materials properties variability. As such, any unwanted or unmodeled deviation from the ideal model used during the design phase can be embraced as a parametric uncertainty. Here parametric uncertainty is modeled using sensitivity functions, which provide a clear and direct way of measuring the impact of a parameter deviation on the properties of the system under investigation. Sensitivity functions are of straightforward formulation whenever an analytic dynamic model is available for the system under investigation. Furthermore, they are defined and used outside any probabilistic framework, thus they do not require the explicit definition of a probabilistic model of the uncertainty sources. As such, they can cover a rather large field of applications.

Let us assume, without loss of generality, that the mass and stiffness matrices depend on a set of n_p parameters $\boldsymbol{\vartheta} = [\vartheta_1, \dots, \vartheta_{n_p}] \in \mathbb{R}^{n_p}$. The computation of partial derivative of Eq. (8) with respect to the j-th parameter ϑ_j leads to:

$$\left(-\frac{\partial\omega_{n,i}^2}{\partial\vartheta_j}\mathbf{M}(\boldsymbol{\vartheta}) - \omega_{n,i}^2\frac{\partial\mathbf{M}(\boldsymbol{\vartheta})}{\partial\vartheta_j} + \frac{\partial\mathbf{K}(\boldsymbol{\vartheta})}{\partial\vartheta_j}\right)\mathbf{u}_i + \left(-\omega_{n,i}^2\mathbf{M}(\boldsymbol{\vartheta}) + \mathbf{K}(\boldsymbol{\vartheta})\right)\frac{\partial\mathbf{u_i}}{\partial\vartheta_j} = \mathbf{0} \tag{9}$$

The premultiplication of the left-hand side of Eq. (9) by $\mathbf{u}_i^T$ enables to simplify its second term since Eq. (8) reveals that $\mathbf{u}_i^T\left(-\omega_{n,i}^2\mathbf{M} + \mathbf{K}\right) = \mathbf{0}$ for $i = 1, \dots, N$, hence a more compact form for Eq. (9) is obtained:

$$\mathbf{u}_i^T\left(-\frac{\partial\omega_{n,i}^2}{\partial\vartheta_j}\mathbf{M}(\boldsymbol{\vartheta}) - \omega_{n,i}^2\frac{\partial\mathbf{M}(\boldsymbol{\vartheta})}{\partial\vartheta_j} + \frac{\partial\mathbf{K}(\boldsymbol{\vartheta})}{\partial\vartheta_j}\right)\mathbf{u}_i = 0 \tag{10}$$

Finally, the impact of the deviation of the j-th parameter ϑ_j on the i-th natural frequency $\omega_{n,i}$ is captured by the sensitivity function $S_{i,j}$, which can be inferred through some manipulations from Eq. (10), and is defined as:

$$S_{i,j} = \frac{\partial\omega_{n,i}^2}{\partial\vartheta_j} = \frac{\mathbf{u}_i^T\left(-\omega_{n,i}^2\frac{\partial\mathbf{M}(\boldsymbol{\vartheta})}{\partial\vartheta_j} + \frac{\partial\mathbf{K}(\boldsymbol{\vartheta})}{\partial\vartheta_j}\right)\mathbf{u}_i}{\mathbf{u}_i^T\mathbf{M}(\boldsymbol{\vartheta})\mathbf{u}_i} \tag{11}$$

2.3. Structural modification for the assignment of natural frequencies and mode shapes

The formulation in Eq. (8) is particularly useful to formulate an Inverse Dynamic Structural Modification problem [39], which consists in computing the modification matrices $\Delta\mathbf{M} \in \mathbb{R}^{N\times N}$ and $\Delta\mathbf{K} \in \mathbb{R}^{N\times N}$ that assign the n_d desired eigenpairs denoted by $(\bar{\omega}_{n,i}, \bar{\mathbf{u}}_\mathbf{i})$, with $i = 1, \dots, n_d$. The IDSM is cast as:

$$\left(-\bar{\omega}_{n,i}^2(\mathbf{M} + \Delta\mathbf{M}) + \mathbf{K} + \Delta\mathbf{K}\right)\bar{\mathbf{u}}_i = \mathbf{0} \quad \text{with} \quad i = 1, \dots, n_d \tag{12}$$

The solvability of Eq. (12) is not ensured for all the choice of the modification matrices. In particular, let us assume that n_x design variables, collected in $\mathbf{x} = [x_1, \dots, x_{n_x}] \in \mathbb{R}^{n_x}$, are employed to modify the system. The topology of the modification matrices as well as the rank of the modification, which is lower or equal to n_x, influence the assignability of the prescribed eigenpairs. In principle, one natural frequency is assignable by means of one independent design variable in accordance with the rank requirement principle [51]. In practice, two issues arise: first, the rank requirement principle does not ensure the attainability of the desired mode shape [52]. Secondly, technological and economical constraints limit the admissible magnitude for the design variables and hence the achievement of the prescribed eigenstructure. Lower and upper bounds, respectively denoted by $\mathbf{x}^L$ and $\mathbf{x}^U$, are here employed to constrain the design variables. More general constraints can be introduced to ensure the fulfillment of other design necessities as well: it is assumed here that such constraints can be represented as linear equality constrains as $\mathbf{Ax} = \mathbf{b}$, with $\mathbf{A} \in \mathbb{R}^{n_g\times n_x}$ and $\mathbf{b} \in \mathbb{R}^{n_g}$. The IDSM is recast, therefore, as follows:

$$\begin{aligned} \min_{\mathbf{x}} \quad & \sum_{i=1}^{n_d}\left\|\left(-\bar{\omega}_{n,i}^2(\mathbf{M} + \Delta\mathbf{M}(\mathbf{x})) + \mathbf{K} + \Delta\mathbf{K}(\mathbf{x})\right)\bar{\mathbf{u}}_i\right\|_2^2 \\ \text{s.t.} \quad & \mathbf{x}^L \le \mathbf{x} \le \mathbf{x}^U \quad \cup \quad \mathbf{Ax} = \mathbf{b} \end{aligned} \tag{13}$$

This formulation is suitable for all cases in which n_d eigenpairs are to be assigned, however such formulation can be extended to the more general case of partial assignment problems, according to the developments presented in [35,53]. According to this framework, eigenpairs entries can be either assigned to a specific value, to a defined domain, or let unassigned. A partial assignment counterpart of Eq. (13) is here defined by including the additional inequality constraint $\mathbf{u}_i^L \le \mathbf{u}_i \le \mathbf{u}_i^u$ to Eq. (13).

2.4. Robust assignment of the natural frequencies

Sensitivity functions can be used to embed a robustness constraint in the formulation of the assignment problem. In particular, the aim here is to ensure that the assigned frequencies are minimally sensitive to parametric deviations, as any alteration of the prescribed natural frequencies result in a significant degradation of the free response of the system. In the case under consideration, this phenomenon can be measured by evaluating the amplitude of residual vibrations in a rest-to-rest motion task.

In this work it is assumed that a subset of the natural frequencies $\omega_{n,i}$, together with their mode shapes $\mathbf{u_i}$, can be altered to improve the dynamic behavior of the system, according to a structural modification procedure that is introduced in the following sections. The desired sensitivity $\bar{S}_{i,j}$ of the i-th prescribed natural frequency with respect to the j-th physical parameter is described by:

$$\bar{S}_{i,j} = \frac{\partial\bar{\omega}_{n,i}^2}{\partial\vartheta_j} = \frac{\bar{\mathbf{u}}_i^T\left(-\bar{\omega}_{n,i}^2\mathbf{J}_{\mathbf{M}+\Delta\mathbf{M}}^{\boldsymbol{\vartheta}_\mathbf{j}} + \mathbf{J}_{\mathbf{K}+\Delta\mathbf{K}}^{\boldsymbol{\vartheta}_\mathbf{j}}\right)\bar{\mathbf{u}}_i}{\bar{\mathbf{u}}_i^T\left(\mathbf{M}(\boldsymbol{\vartheta}) + \Delta\mathbf{M}(\mathbf{x}, \boldsymbol{\vartheta})\right)\bar{\mathbf{u}}_i} \tag{14}$$

where the Jacobian matrices for the modified system are:

$$\begin{aligned} \mathbf{J}_{\mathbf{M}+\Delta\mathbf{M}}^{\boldsymbol{\vartheta}_\mathbf{j}} &= \frac{\partial\left(\mathbf{M}(\boldsymbol{\vartheta}) + \Delta\mathbf{M}(\mathbf{x}, \boldsymbol{\vartheta})\right)}{\partial\vartheta_j} \\ \mathbf{J}_{\mathbf{K}+\Delta\mathbf{K}}^{\vartheta_j} &= \frac{\partial\left(\mathbf{K}(\boldsymbol{\vartheta}) + \Delta\mathbf{K}(\mathbf{x}, \boldsymbol{\vartheta})\right)}{\partial\vartheta_j} \end{aligned} \tag{15}$$

Eq. (14) is recast, in a more compact non-fractional form into:

$$\bar{\boldsymbol{\Phi}}_{i,j}(\mathbf{x}, \boldsymbol{\vartheta}, \bar{\mathbf{u}}_i) = 0 \tag{16}$$

where:

$$\begin{aligned} N_{i,j}(\mathbf{x}, \boldsymbol{\vartheta}, \bar{\mathbf{u}}_i) &= \bar{\mathbf{u}}_i^T\left(-\bar{\omega}_{n,i}^2\mathbf{J}_{\mathbf{M}+\Delta\mathbf{M}}^{\vartheta_j} + \mathbf{J}_{\mathbf{K}+\Delta\mathbf{K}}^{\boldsymbol{\vartheta}_\mathbf{j}}\right)\bar{\mathbf{u}}_i \\ D_{i,j}(\mathbf{x}, \boldsymbol{\vartheta}, \bar{\mathbf{u}}_i) &= \bar{\mathbf{u}}_i^T\left(\mathbf{M}(\boldsymbol{\vartheta}) + \Delta\mathbf{M}(\mathbf{x}, \boldsymbol{\vartheta})\right)\bar{\mathbf{u}}_i \\ \bar{\boldsymbol{\Phi}}_{i,j}(\mathbf{x}, \boldsymbol{\vartheta}, \bar{\mathbf{u}}_i) &= D_{i,j}(\mathbf{x}, \boldsymbol{\vartheta}, \bar{\mathbf{u}}_i)\bar{S}_{i,j} - N_{i,j}(\mathbf{x}, \boldsymbol{\vartheta}, \bar{\mathbf{u}}_i) \end{aligned} \tag{17}$$

Eq. (16) can then be formulated for the assignment of n_s prescribed sensitivities with respect to different parameters and for n_d desired natural frequencies, leading to the general form:

$$\underbrace{\begin{bmatrix} \bar{\boldsymbol{\Phi}}_{1,1}(\mathbf{x}, \boldsymbol{\vartheta}, \bar{\mathbf{u}}_1) & \cdots & \bar{\boldsymbol{\Phi}}_{1,n_d}(\mathbf{x}, \boldsymbol{\vartheta}, \bar{\mathbf{u}}_{n_d}) \\ \vdots & \bar{\boldsymbol{\Phi}}_{i,j}(\mathbf{x}, \boldsymbol{\vartheta}, \bar{\mathbf{u}}_i) & \vdots \\ \bar{\boldsymbol{\Phi}}_{n_s,1}(\mathbf{x}, \boldsymbol{\vartheta}, \bar{\mathbf{u}}_1) & \cdots & \bar{\boldsymbol{\Phi}}_{n_s,n_d}(\mathbf{x}, \boldsymbol{\vartheta}, \bar{\mathbf{u}}_{n_d}) \end{bmatrix}}_{=\bar{\boldsymbol{\Phi}}(\mathbf{x}, \boldsymbol{\vartheta}, \bar{\mathbf{u}}) \in \mathbb{R}^{n_s\times n_d}} = 0 \tag{18}$$

Eq. (18) enables to embed the robustness constraint, as well as the partial assignment of eigenvectors, into Eq. (13), ensuring that prescribed sensitivity values are achieved. The least-square problem in Eq. (13) can therefore be recast for the case of robust partial assignment

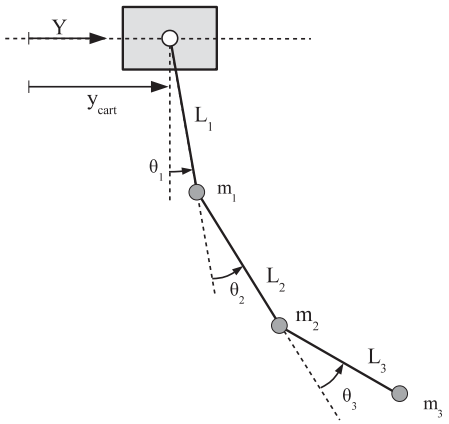

Fig. 1. Sketch of the triple pendulum.

of the natural frequencies as follows:

$$\begin{aligned} \min_{\mathbf{x}} \quad & \sum_{i=1}^{n_d} \left\| \left(-\bar{\omega}_{n,i}^2 \left(\mathbf{M}(\boldsymbol{\vartheta}) + \Delta\mathbf{M}(\boldsymbol{\vartheta}, \mathbf{x}) \right) + \mathbf{K}(\boldsymbol{\vartheta}) + \Delta\mathbf{K}(\boldsymbol{\vartheta}, \mathbf{x}) \right) \bar{\mathbf{u}}_\mathbf{i} \right\|_2^2 \\ \text{s.t.} \quad & \mathbf{x}^L \le \mathbf{x} \le \mathbf{x}^U \quad \cup \quad \mathbf{A}\mathbf{x} = \mathbf{b} \\ & \mathbf{u}_\mathbf{i}^L \le \mathbf{u}_\mathbf{i} \le \mathbf{u}_\mathbf{i}^U \\ & \bar{\boldsymbol{\Phi}}(\mathbf{x}, \boldsymbol{\vartheta}, \bar{\mathbf{u}}) = 0 \end{aligned} \tag{19}$$

An application of the proposed robust IDSM technique to a benchmark problem is provided in the next section.

3. Numerical assessment

3.1. Dynamic model of the triple pendulum

Let us consider a triple pendulum on a cart, as sketched in Fig. 1, made by the suspended masses m_1, m_2 and m_3 and by the massless cable lengths l_1, l_2 and l_3. Its dynamic model can be obtained through the Euler–Lagrange formulation [54], which can then be linearized around its stable equilibrium position. The equation of motion of the undamped triple pendulum, in the case of small oscillations, takes the following form:

$$\mathbf{M} \begin{bmatrix} \ddot{\vartheta}_1(t) \\ \ddot{\vartheta}_2(t) \\ \ddot{\vartheta}_3(t) \end{bmatrix} + \mathbf{K} \begin{bmatrix} \vartheta_1(t) \\ \vartheta_2(t) \\ \vartheta_3(t) \end{bmatrix} = \mathbf{B}\ddot{y}_{\text{cart}}(t) \tag{20}$$

where the mass, stiffness and actuation matrices are respectively defined as:

$$\begin{aligned} \mathbf{M} &= \begin{bmatrix} m_1 L_1 & m_2 L_1 & m_3 L_1 \\ 0 & m_2 L_2 & m_3 L_2 \\ 0 & 0 & m_3 L_3 \end{bmatrix} \begin{bmatrix} L_1 & 0 & 0 \\ L_1 & L_2 & 0 \\ L_1 & L_2 & L_3 \end{bmatrix} \\ \mathbf{K} &= g \begin{bmatrix} m_1 + m_2 + m_3 & 0 & 0 \\ 0 & m_2 + m_3 & 0 \\ 0 & 0 & m_3 \end{bmatrix} \begin{bmatrix} L_1 & 0 & 0 \\ 0 & L_2 & 0 \\ 0 & 0 & L_3 \end{bmatrix} \\ \mathbf{B} &= -\begin{bmatrix} (m_1 + m_2 + m_3) L_1 \\ (m_2 + m_3) L_2 \\ m_3 L_3 \end{bmatrix} \end{aligned} \tag{21}$$

being $\boldsymbol{\vartheta} = [\vartheta_1, \vartheta_2, \vartheta_3]^T$ the vector of the relative sway angles, as defined in Fig. 1. The exogenous input is assumed to be the acceleration of the cart, $\ddot{y}_{cart}$.

Despite its perceived simplicity, the model under investigation poses some challenges, mainly due to the non-obvious and analytically complex relationship between the physical parameters, i.e. the cable lengths and the mass weights, and the resulting eigenstructure. Nonetheless, the model is characterized by its three oscillating frequencies, which are listed in Table 1. The model is assumed to be undamped, following an hypothesis that is well supported by the experimental results obtained using the laboratory setup that will be presented in the next section. Nonetheless, damping can still be included by a slight revision of the formulation of Eq. (20) whenever needed.

Table 1
Original system parameters.

Parameter	Value	Unit
m_1	0.1016	[kg]
m_2	0.1074	[kg]
m_3	0.1092	[kg]
L_1	0.3487	[m]
L_2	0.3394	[m]
L_3	0.3336	[m]
$L_1 + L_2 + L_3$	1.0217	[m]
g	9.80655	[ms^{-2}]
$\omega_{n,1}$	3.45	[rads^{-1}]
$\omega_{n,2}$	8.22	[rads^{-1}]
$\omega_{n,3}$	13.71	[rads^{-1}]

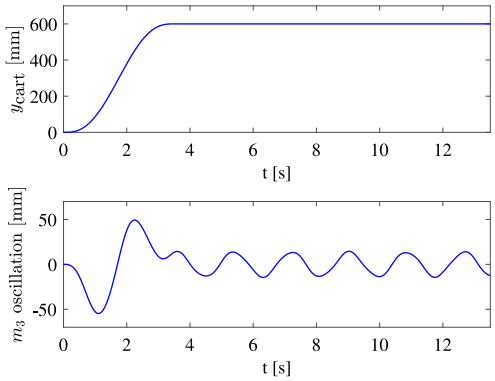

Fig. 2. Unshaped fifth-degree polynomial trajectory and oscillations of mass m_3.

Underactuation combined with the pronounced system flexibility deteriorate the performances of this system in executing point-to-point motion tasks when high dynamics is required. To show and quantify such phenomenon, the triple pendulum is simulated while the cart is performing a fifth-degree polynomial motion profile. The motion is chosen so that initial and final acceleration of the cart can be set to zero, i.e. a rest-to-rest motion is performed, and to achieve a displacement of the cart equal to *0.6* m in *3.5* s. The motion profile is shown on top-half of Fig. 2: its execution results in the oscillation of mass m_3 shown in the graph on the bottom of the same figure.

The simulation highlights the large amplitude of the residual oscillation that can happen whenever a generic motion profile is used.

Since the triple pendulum exhibits three natural frequency, a cascade of three ZV and of three ZVD shapers are either applied to the original unshaped motion profile shown in 2, leading to the results shown in Figs. 3 and 4, which highlight the capability of both methods to cancel residual vibrations under nominal conditions. In all cases the duration of the original (unshaped) motion profile is pre-compensated by shorting it, to ensure that the shaped motion, in all cases, lasts precisely 3.5 s.

In this paper the ZV and ZVD shapers are employed for the numerical investigation and in the experimental campaign as well, given that such methods ensure that residual vibrations are canceled whenever the eigenstructure of the system is as predicted. Accordingly, the amplitude of residual vibrations will be used to indirectly quantify the alteration

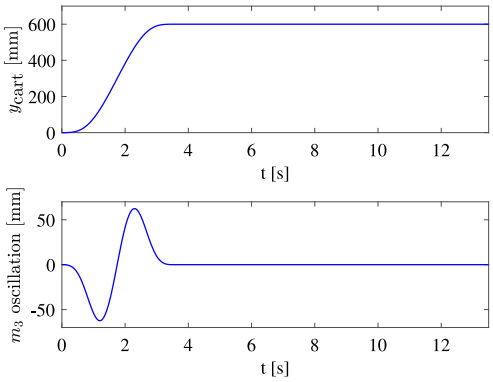

Fig. 3. ZV shaped fifth-degree polynomial trajectory and oscillations of mass m_3, nominal system.

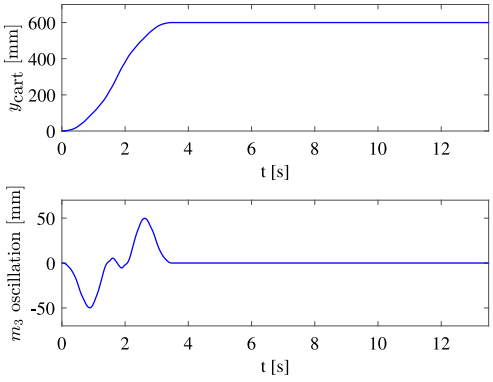

Fig. 4. ZVD shaped fifth-degree polynomial trajectory and oscillations of mass m_3, nominal system.

of the natural frequencies with, and without, the application of the proposed robust IDSM method.

3.2. Robust assignment of the natural frequencies for the triple pendulum

As already mentioned in the previous section, input shapers performance deteriorates if the model does not correctly describe the physical plant, i.e. if incorrect natural frequencies are adopted to tune the shapers. In this paper, for fairness of comparison with respect to the original system, the robust assignment method described in Section 2.4 is exploited to keep unchanged the lowest natural frequency of the triple pendulum and to increase its robustness to variations of mass m_3. In this example the target of the structural modification is to reduce the sensitivity $\partial\omega_{n,1}^2/\partial m_3$ by 40%. The admissible modifications are collected in the vector $\mathbf{x} = [\Delta m_1, \Delta m_2, \Delta L_1, \Delta L_2, \Delta L_3]$, bounds on the design variables are reported in Table 2. The latter are defined in compliance with some technical limitations of the available experimental setup. The modification of mass m_3 is not admitted for a fair comparison between the original and the modified system, given that m_3 is the parameter to be artificially altered to modify the modal properties of the triple pendulum. An additional constraint is introduced to ensure that the total length of the pendulum, i.e. $L_1 + L_2 + L_3$, is kept unchanged, again, to ensure a fair comparison. The different scenario of a single pendulum with a time-varying cable length has been tackled in [55] through an active control strategy.

The inverse dynamic structural modification problem of Eq. (19) is solved through a custom MATLAB routine, bases on the solver *fmincon*, which can handle nonlinearities both in the cost-function and in the constraints: the convergence to a robust solution for the constrained optimization is achieved by setting as initial guess the original design of the system, i.e. $\mathbf{x_0} = [0, 0, 0, 0, 0]$.

Table 2
Original and modified system parameters and design variables constraints.

Parameter	Unit	Original system	Modification bounds	Modified system
m_1	[kg]	0.1016	[0.0508; 0.4062]	0.1773
m_2	[kg]	0.1074	[0.0537; 0.4297]	0.2688
m_3	[kg]	0.1092	–	0.1902
L_1	[m]	0.3487	[0.0697; 0.6973]	0.4796
L_2	[m]	0.3394	[0.0679; 0.6787]	0.3614
L_3	[m]	0.3336	[0.0667; 0.6673]	0.1808
$L_1 + L_2 + L_3$	[m]	1.0217	–	1.0217

Table 3
Original and modified system natural frequencies and sensitivity of interest.

Parameter	Unit	Original system	Desired value	Modified system
$\omega_{n,1}$	[rads^{-1}]	3.45	3.45	3.45
$\omega_{n,2}$	[rads^{-1}]	8.22	–	8.61
$\omega_{n,3}$	[rads^{-1}]	13.71	–	12.26
$\frac{\partial\omega_{n,1}^2}{m_3}$	[rad^{2}s^{-2}kg^{-1}]	−12.70	−7.62	−7.68

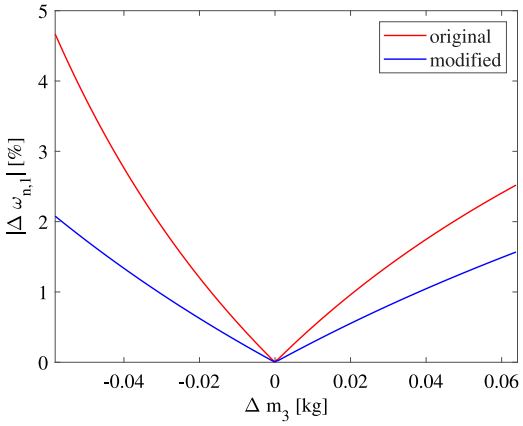

Fig. 5. Percentage variation of $\omega_{n,1}$ vs mass m_3 perturbations: original and modified system. (For interpretation of the references to color in this figure legend, the reader is referred to the web version of this article.)

The original system and modified system natural frequencies, together with the sensitivity of interest, are reported in Table 3 and corroborate the fulfillment of the prescribed assignment task: the first natural frequency is unaltered and the actual sensitivity reduction is equal to 39.5%, which is very close to the target value. To better quantify the robustness enhancement brought by the sensitivity reduction, the percentage variation of the first natural frequency with respect to variations of m_3 are shown in Fig. 5: the red plot refers to the nominal system, the blue plot to the system modified according to the results of the IDSM routine.

Fig. 5 shows that, after the structural modification, the amplitude of the alteration of $\omega_{n,1}$ resulting from a given alteration of m_3 is roughly divided by two. It must be highlighted that the level of reduction can be defined by the user according to the specific requirements of the application, since lower target sensitivities result in smaller perturbations of $\omega_{n,1}$ for equal mass modifications.

3.3. Comparison of the original and modified system response after perturbation

The increase of robustness is assessed in this section by comparing the residual vibration of the original and modified triple pendulum when mass m_3 is perturbed in the interval $[-53.3\%; +58.8\%]$ with respect

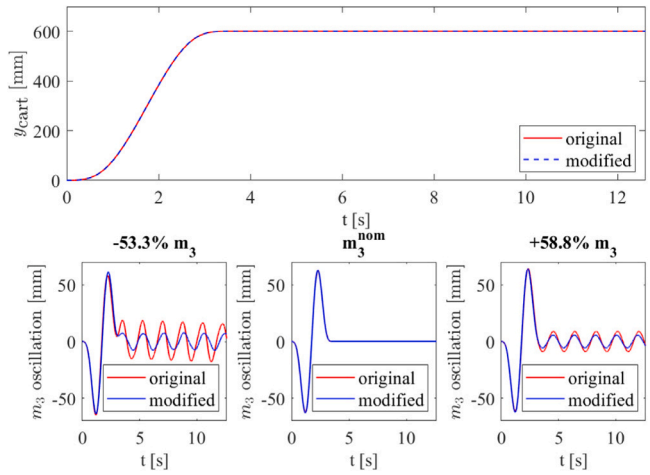

Fig. 6. ZV shaper: comparison of m_3 oscillations the nominal system and for extreme m_3 perturbations. (For interpretation of the references to color in this figure legend, the reader is referred to the web version of this article.)

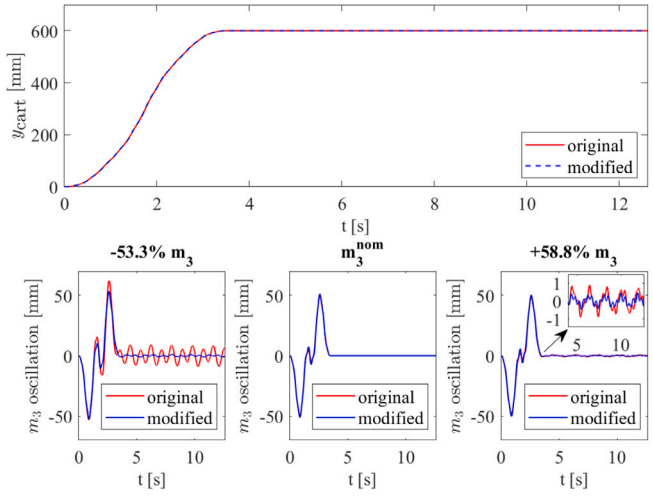

Fig. 7. ZVD shaper: comparison of m_3 oscillations for the nominal system and for extreme m_3 perturbations. (For interpretation of the references to color in this figure legend, the reader is referred to the web version of this article.)

to its nominal value, and both the ZV and ZVD shapers are tuned by considering the nominal system natural frequencies. The residual vibration of the original and modified systems when using the ZV shaper are shown in Fig. 6 for the nominal system and for the maximum positive and negative perturbations of m_3. A similar analysis is proposed in Fig. 7 for the ZVD shaper as well. As expected, robustness is increased by taking advantage of the ZVD shaper instead of the ZV shaper. However, the robustness of the system to variations of m_3 is further increased by the inclusion of the robustifying structural modification for both shapers since the amplitude of the oscillations shown with a blue line is always smaller than the one represented by the red line, the latter being referred to the system prior to the structural modifications. This feature provides a confirmation of the usefulness of structural modification in assigning modal properties that are minimally affected by perturbations. It should also be noted that, at the same time, perfect residual oscillation is retained in the case of null perturbations, as it can be seen from the center plot of both Figs. 6 and 7.

Furthermore, Table 4 shows the peak-to-peak residual vibration magnitude obtained through numerical simulations for five different values of Δm_3, taking into consideration, again, the ZV and ZVD shapers and both the nominal and the modified pendulums. The same analysis

Table 4
Residual oscillation of mass m_3 for the original and modified system: ZV and ZVD shapers, numerical results.

Δm_3	ZV Shaper residual oscillation			ZVD Shaper residual oscillation		
	Original	Modified	Reduction	Original	Modified	Reduction
[kg]	[mm]	[mm]	[%]	[mm]	[mm]	[%]
−0.0582	37.5	15.7	58.0	18.5	2.2	88.3
−0.0291	14.3	6.9	51.6	2.5	0.4	85.2
0	0	0	–	0	0	–
+0.0351	11.1	6.6	40.4	1.0	0.3	65.3
+0.0642	17.8	11.2	37.0	1.8	0.9	48.6

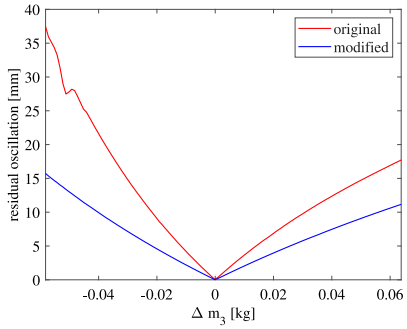

Fig. 8. ZV shaper: comparison of peak-to-peak residual vibration amplitude vs mass m_3 perturbation, numerical results.

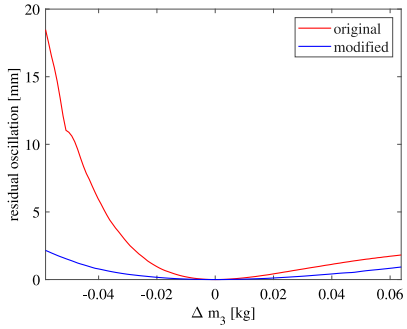

Fig. 9. ZVD shaper: comparison of peak-to-peak residual vibration amplitude vs mass m_3 perturbation, numerical results.

will be performed in the experiments whose results are provided in the next section. The data in Table 4 show that the structural modification can, at least in a numerical environment, reduce the residual vibration amplitude resulting from a mass perturbation, by a percentage that varies between 37% and 88.3%, which is an impressive feature considering the scale of the perturbation.

Figs. 8 and 9 show the amplitude of peak-to-peak residual vibrations for a continuous set of perturbation of m_3 in the $[-53.3\%, +58.8\%]$ range. The results confirm the consistency of the robustness improvement over the considered range of perturbations.

It must be also pointed out that the robustness enhancement brought by the robust IDSM cannot always be obtained by the simple enhancement of the motion profile, since the application of shapers with increased robustness is not always trivial or practically feasible. Let us consider, for example, the application of the ZVDD shaper introduced in Section 2.1 to the test-case under consideration. The 'double-robust' suppression of each mode enforces the introduction of a delay equal to $3\tau_d$, which results in a total delay equal to 4.57 s. This amount of delay is incompatible to the motion execution time adopted so far, i.e. 3.5 s, therefore longer execution times must be accepted. As a matter of example, let us define a total motion time equal to 5 s,

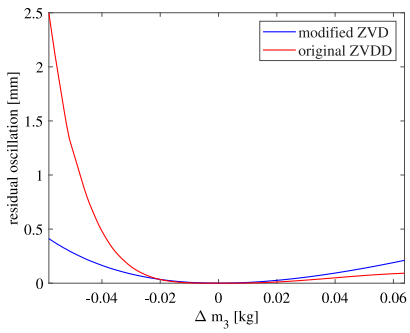

Fig. 10. Comparison of peak-to-peak residual vibration amplitude vs mass m_3 perturbation for the ZVDD on the original and the ZVD on the modified system, numerical results.

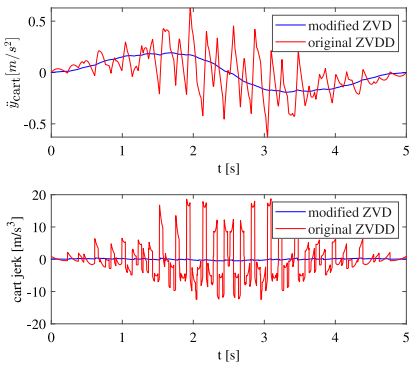

Fig. 11. Cart acceleration and jerk comparison for the ZVDD shaper in the original system and the ZVD shaper in the modified system, numerical results. (For interpretation of the references to color in this figure legend, the reader is referred to the web version of this article.)

and let us compare the results of two numerical test-cases: in the first one the original pendulum is moved over a profile altered by a ZVDD shaper, while in the second one the modified pendulum and the simpler ZVD shaper are used together. This simple experiment provides a direct measure of which method is more effective: the 'robustification' of the ZVD shaper, or the 'robustification' of the IDSM method. The analysis is repeated over the usual range of perturbation of m_3, and the peak-to-peak amplitude of the residual vibration are shown in Fig. 10. The figure highlights that the robustness-enhanced ZVDD shaper has a slightly better performance for positive perturbations and a significantly worse performance whenever mass m_3 is reduced.

However, this numerical results would be hard to match in an actual experiment, as the motion profile resulting from the application of the ZVDD shaper is the one shown, in terms of cart acceleration and jerk, in Fig. 11 by the red line. The execution of such a motion profile would require an unusually high bandwidth of the motion control loop. Indeed, relying on structural modification to enhance the robustness of the ZVD solution does not alter so dramatically peak jerk and acceleration, as shown in Fig. 11. In detail, the absolute maximum and the RMS acceleration are respectively: 0.63 m/s^2 and 0.19 m/s^2 in the first case and 0.19 m/s^2 and 0.13 m/s^2 in the second case. In terms of maximum and RMS jerk, the respective values are 18.7 m/s^3 and 5.9 m/s^3, with the ZVDD shaper, and 0.6 m/s^3 and 0.2 m/s^3 with the ZVD shaper and the structural modification.

This experiment has shown that the enhancement of the robustness by just acting on the design of the shaper is not theoretically advantageous, nor technically feasible, considering the extreme high-frequency content of the acceleration and motion profiles shown in Fig. 11.

Fig. 12. The experimental setup.

4. Experimental results

This section collects the results of the application of the proposed method to an experimental setup which comprises either the nominal or the modified triple pendulum, whose actuation is provided by an Adept Quattro s650 h robot. The linear motion of the end effector is meant to replicate the motion of the cart idealized in Fig. 1. A picture of the manipulator used for the tests, together with the triple pendulum, is shown in Fig. 12. The robot is controlled by the proprietary Adept SmartController, and is programmed to execute a user-defined trajectory.

The motion of the pendulum is measured using a motion capture system developed by Vicon, which uses four high-speed cameras to reconstruct the position of some markers which are located on the robot end-effector and on mass m_3. The system allows the measurement of the spatial position of these two object with a sampling frequency up to 400 Hz and with sub-millimeter accuracy [56].

The experiments have reproduced all the test designed for the numerical investigation, in order to provide a full validation of the robust structural modification procedure.

4.1. Nominal plant

The tests performed on the experimental plant mimic, as already mentioned, all the numerical tests already performed for the preliminary validation of the proposed model. In particular, a first test campaign has been conducted on the 'nominal' pendulum, i.e. the system in which the system parameters L_i and m_i take their initial, non-optimized, values.

The execution of the motion profile after the application of both the ZV and the ZVD shapers produces the results shown in Fig. 1, where the red lines separate, in the graph on the bottom, initial, transients and residual vibrations.

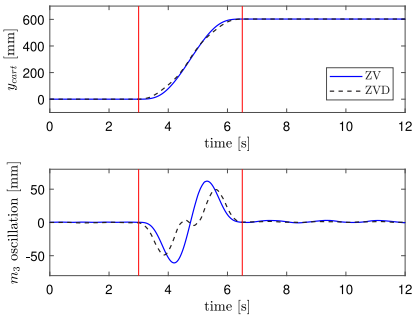

Fig. 13. Application of the ZV and ZVD shapers to the nominal, unperturbed pendulum: experimental results. (For interpretation of the references to color in this figure legend, the reader is referred to the web version of this article.)

Fig. 13 shows in the upper graph the position of the cart, which provides a total displacement equal to 0.6 m in 3.5 s, while the lower graphs shows the longitudinal displacement of mass m_3, measured in mm. Despite the application of a properly tuned cascade of ZV shapers, the amplitude of the residual oscillation of the third mass of the pendulum is not zero: this is due mainly to the non-perfect reproduction of the prescribed trajectory by the robot end-effector. Despite the high-speed capabilities of the robot, it cannot provide perfect trajectory tracking since the robot controller does not support the execution of arbitrary motion profile: hence the desired motion profiles has to be re-interpolated according to the motion primitives natively supported by the robot. This re-sampling happens with a refresh frequency equal to 32 Hz, with a consequent slight, but noticeable, distortion of the motion profile. The main effect of this distortion, which can be modeled as an external disturbance, is the accentuation of the residual vibrations shown in Fig. 13, whose amplitude is roughly equal to 2 mm peak-to-peak. Other sources of uncertainties are the imperfect matching between the actual oscillating modes and the modeled ones, which differ in the order of tents of Hz, as well as the imperfect planarity of the motion of the robot and of the pendulum. While these effects are detectable, they still are overshadowed by the robot inaccuracy in reproducing the prescribed speed profile.

The application of the ZVD-shaped motion profile to the same system results in a slightly smaller residual vibration amplitude, which, averaged over several tests, is equal to a peak-to-peak amplitude equal to 1.2 mm. This improved result is due to the inherent reduced sensitivity to the motion profile disturbances as the result of the improved robustness brought by the use of the ZVD shaper.

4.2. Perturbed plant

In order to provide a more comprehensive evaluation of the effective robustness, again through the measurement of residual vibrations amplitude, the ZV and ZVD shaped motion profiles have been applied to the non-optimized pendulum with a discrete set of 4 possible modification to mass m_3, obtained by adding or subtracting a specific mass value, reproducing to the same perturbations tested on the numerical model and listed as Δm_3 in Table 4.

Fig. 14 shows the outcome of the application of the ZV-shaped motion profile on the oscillations of mass m_3: the plot in the center refers to the unperturbed pendulums, while the one on the left and on the right refer to the pendulums with maximum negative and positive Δm_3, i.e. −53.3% and +58.8%, respectively. The red lines refer to the original pendulum, the blue lines to the robustified one. Such plots are the results of the experimental reproduction of the numerical tests whose results are reported in Fig. 6. The numerical results of Fig. 6 are well supported by the experimental results: the 'robustification' operated to the pendulum through the structural modification does effectively produce a significant improvement in terms of residual

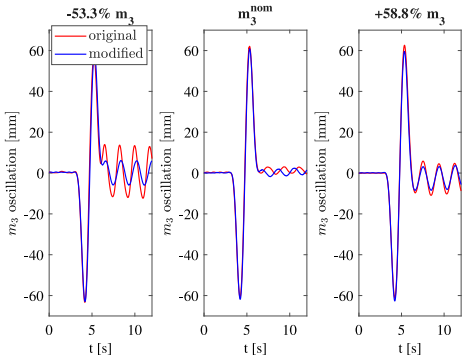

Fig. 14. ZV shaper: comparison of m_3 oscillations for the nominal system and for extreme m_3 perturbations, experimental results. (For interpretation of the references to color in this figure legend, the reader is referred to the web version of this article.)

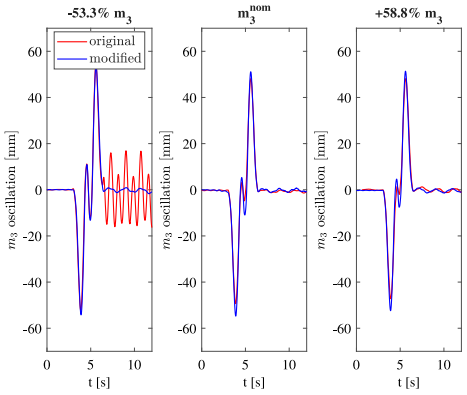

Fig. 15. ZVD shaper: comparison of m_3 oscillations for the nominal system and for extreme m_3 perturbations, experimental results. (For interpretation of the references to color in this figure legend, the reader is referred to the web version of this article.)

oscillation amplitude, which is more noticeable when reducing mass m_3 rather than increasing, as in the case of the left-side graph of Fig. 14 vs. the right-side one. These results are expected, since it has indeed already been shown, in Fig. 5, that negative alterations to mass m_3 provide a larger perturbation on the first oscillating mode, $\omega_{n,1}$, than positive ones of the same magnitude.

Repeating the same tests with a different motion profile, i.e. the one generated by the ZVD filtering of the quintic polynomial profile, produces the results reported in Fig. 15. The graphs show that, as predicted by Fig. 7, residual vibrations are confined to small values for the unperturbed case and for the positive mass m_3 perturbation, and in such conditions the structural modification process provides a limited improvement over the one already brought by the robustification introduced by the enhanced motion profile. The case of maximum reduction of mass m_3, as shown in the plot on the left-side of Fig. 15, showcases the most prominent effect of the robustification provided by the structural modification: the oscillation observed when mass m_3 is reduced by more than half is changed from 18.5 mm to just 2.2 mm. In all, it can be observed that the structural modification takes care of reducing the residual oscillation amplitude when the robust shaper cannot.

A condensed representation of the results, formulated in terms of peak-to-peak amplitude of residual oscillation are reported in Figs. 16 and 17 (which are the experimental counterparts of Figs. 8 and 9, respectively) and in Table 5. The data in Table 5 are shown as mean values over 5 experimental trial for each entry of the table.

In Fig. 14 and in Fig. 15 as well, the blue lines lie always below the red lines, meaning the porpoised structural modification is proved to

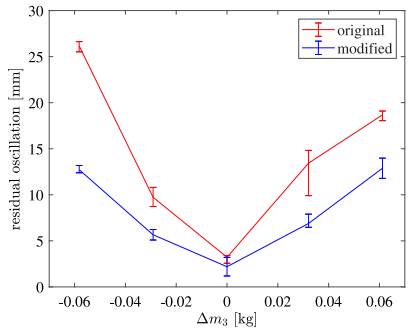

Fig. 16. ZV shaper: comparison of residual vibration vs mass m_3 perturbation.

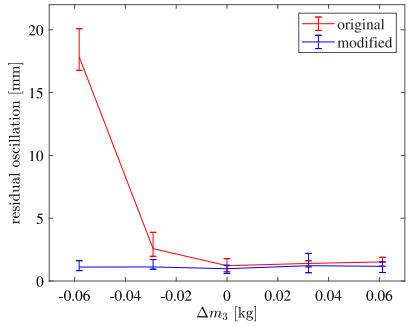

Fig. 17. ZVD shaper: comparison of residual vibration vs mass m_3 perturbation.

Table 5
Residual oscillation of mass m_3 for the original and modified system: ZV and ZVD shapers, experimental results.

Δm_3	ZV Shaper residual oscillation			ZVD Shaper residual oscillation		
	Original	Modified	Reduction	Original	Modified	Reduction
[kg]	[mm]	[mm]	[%]	[mm]	[mm]	[%]
−0.0582	26.2	12.7	51.5	17.8	1,1	93.8
−0.0291	9.7	5.7	41.2	2.5	1.1	56.0
0	3.2	2.2	31.3	1.2	1.0	8.3
+0.0351	13.4	6.9	48.5	1.4	1.2	14.3
+0.0642	18.7	12.9	31.0	1.5	1.2	20.0

be beneficial in enhancing parametric robustness over a wide range of perturbations. The imprecision in the achievement of true zero residual vibrations in the nominal cases is reputed to be mainly due to the less than perfect execution of the planned motion profile.

The numbers in Table 5 clearly show the improvement brought by the structural modifications: the reduction of the residual vibration amplitude, in percentage, ranges from 31% to 51.5% when using the ZV shaper. The reduction observed for the robust motion profile as the results of the structural modification vary over a wider range: in the unperturbed case it is as low as 8%, but it can reach values as high as 93.8%. The inclusion of robustness at both the motion planning level and at the structural modification level result in a heavily desensitized system, in which even large modifications of mass m_3 result in sensibly small residual oscillation, hence the target of improved robustness is met with success.

5. Conclusions

A novel and effective approach to improve the performance of underactuated uncertain flexible system subject to high-dynamic motion is considered. The technique used to achieve zero residual vibrations in rest-to-rest motion under robust conditions, i.e. with minimal sensitivity to the change of one or more physical parameters of the system, is based on the concurrent use of shapers, that might be robust or not, as well as on the use of Inverse Dynamic Structural Modification. The latter, together with the partial eigenstructure assignment paradigm, is exploited to robustly assign the system natural frequencies. To cope with this task, a non-probabilistic robustness constraint, formulated using analytic parametric sensitivities, is embedded in the algorithm that computes the structural modifications.

The proposed method can be applied to a wide range of applications, being suitable to any system represented by a linear, or linearized, dynamic model. The problem is solved through a constrained non-linear non-convex least-square minimization procedure that ensures the technical and economical feasibility of its solution, providing both laboratory and industrial applicability of the proposed mechanical design technique.

Numerical simulations and experimental testing of the proposed technique are provided for a benchmark system composed by a triple pendulum and an Adept Quattro robot whose motion excites the flexible system. Underactuation and flexibility lead to large unwanted residual vibrations that are suppressed by planning the motion alternatively through cascades of ZV or ZVD shapers properly tuned through the natural frequencies of the system.

Both the numerical and experimental tests corroborate the effectiveness of the proposed method in increasing the robustness with respect to variations of the payload mass of the triple pendulum. Hence, the alteration of the dominant natural frequency of the system are reduced with respect to the nominal design of the system, leading to a consistent improvement in the suppression of the residual oscillations of the system when it is subject to high-dynamic trajectories. The proposed method is of very general application, thus it can potentially be adopted, in future works, to other test benches and with other trajectory specifications that may overwhelm the goal of residual vibration damping.

CRediT authorship contribution statement

Paolo Boscariol: Conceptualization, Methodology, Software, Validation, Data curation, Writing – original draft, Writing – review & editing. **Dario Richiedei:** Conceptualization, Methodology, Writing – review & editing. **Iacopo Tamellin:** Conceptualization, Methodology, Software, Validation, Data curation, Writing – original draft, Writing – review & editing.

Declaration of competing interest

The authors declare that they have no known competing financial interests or personal relationships that could have appeared to influence the work reported in this paper.

References

[1] X. He, W. He, Y. Liu, Y. Wang, G. Li, Y. Wang, Robust adaptive control of an offshore ocean thermal energy conversion system, IEEE Trans. Syst. Man Cybern. 50 (2018) 5285–5295.
[2] Z. Zhao, Z. Liu, W. He, K.-S. Hong, H.-X. Li, Boundary adaptive fault-tolerant control for a flexible Timoshenko arm with backlash-like hysteresis, Automatica 130 (2021) 109690.
[3] L. Cui, H. Wang, W. Chen, Trajectory planning of a spatial flexible manipulator for vibration suppression, Robot. Auton. Syst. 123 (2020) 103316.
[4] J. Kim, E.A. Croft, Preshaping input trajectories of industrial robots for vibration suppression, Robot. Comput.-Integr. Manuf. 54 (2018) 35–44.
[5] L. Biagiotti, C. Melchiorri, Optimization of generalized s-curve trajectories for residual vibration suppression and compliance with kinematic bounds, IEEE/ASME Trans. Mechatronics (2020).
[6] C.T. Kiang, A. Spowage, C.K. Yoong, Review of control and sensor system of flexible manipulator, J. Intell. Robot. Syst. 77 (2015) 187–213.
[7] H. Rahimi, M. Nazemizadeh, Dynamic analysis and intelligent control techniques for flexible manipulators: a review, Adv. Robot. 28 (2014) 63–76.
[8] R. Alkhatib, M. Golnaraghi, Active structural vibration control: a review, Shock Vib. Dig. 35 (2003) 367.

[9] P. Balaji, K.K. SelvaKumar, Applications of nonlinearity in passive vibration control: a review, J. Vib. Eng. Technol. (2020) 1–31.
[10] A. Mallick, F. Crasta, V.K.N. Kottur, A review on vibration suppression of flexible structures using piezoelectric actuators, in: Proceedings of International Conference on Intelligent Manufacturing and Automation, Springer, 2020, pp. 713–721.
[11] A. Gasparetto, P. Boscariol, A. Lanzutti, R. Vidoni, Path planning and trajectory planning algorithms: A general overview, Motion Oper. Plan. Robotic Syst. (2015) 3–27.
[12] Y. Fang, J. Hu, W. Liu, Q. Shao, J. Qi, Y. Peng, Smooth and time-optimal S-curve trajectory planning for automated robots and machines, Mech. Mach. Theory 137 (2019) 127–153.
[13] H. Liu, X. Lai, W. Wu, Time-optimal and jerk-continuous trajectory planning for robot manipulators with kinematic constraints, Robot. Comput.-Integr. Manuf. 29 (2013) 309–317.
[14] F. Fahroo, I.M. Ross, Direct trajectory optimization by a Chebyshev pseudospectral method, J. Guid. Control Dyn. 25 (2002) 160–166.
[15] S. Kucuk, Optimal trajectory generation algorithm for serial and parallel manipulators, Robot. Comput.-Integr. Manuf. 48 (2017) 219–232.
[16] A. Abe, An effective trajectory planning method for simultaneously suppressing residual vibration and energy consumption of flexible structures, Case Stud. Mech. Syst. Signal Process. 4 (2016) 19–27.
[17] D.J. Balkcom, M.T. Mason, Time optimal trajectories for bounded velocity differential drive vehicles, Int. J. Robot. Res. 21 (2002) 199–217.
[18] M.P. Kelly, DirCol5i: Trajectory optimization for problems with high-order derivatives, J. Dyn. Syst. Meas. Control 141 (2019).
[19] P. Boscariol, A. Gasparetto, Model-based trajectory planning for flexible-link mechanisms with bounded jerk, Robot. Comput.-Integr. Manuf. 29 (2013) 90–99.
[20] P. Bosetti, E. Bertolazzi, Feed-rate and trajectory optimization for CNC machine tools, Robot. Comput.-Integr. Manuf. 30 (2014) 667–677.
[21] O. Von Stryk, R. Bulirsch, Direct and indirect methods for trajectory optimization, Ann. Oper. Res. 37 (1992) 357–373.
[22] W. Singhose, Command shaping for flexible systems: A review of the first 50 years, Int. J. Precis. Eng. Manuf. 10 (2009) 153–168.
[23] P. Boscariol, D. Richiedei, Robust point-to-point trajectory planning for non-linear underactuated systems: Theory and experimental assessment, Robot. Comput.-Integr. Manuf. 50 (2018) 256–265.
[24] W. Singhose, L. Porter, T. Tuttle, N.C. Singer, Vibration reduction using multi-hump input shapers, J. Dyn. Syst. Meas. Control 119 (1997) 320–326.
[25] J.E. Mottershead, Y.M. Ram, Inverse eigenvalue problems in vibration absorption: passive modification and active control, Mech. Syst. Signal Process. 20 (2006) 5–44.
[26] L.J. Adamson, S. Fichera, B. Mokrani, J. Mottershead, Pole placement in uncertain dynamic systems by variance minimisation, Mech. Syst. Signal Process. 127 (2019) 290–305.
[27] L. Adamson, S. Fichera, J. Mottershead, Receptance-based robust eigenstructure assignment, Mech. Syst. Signal Process. 140 (2020) 106697.
[28] D. Richiedei, I. Tamellin, Active control of linear vibrating systems for antiresonance assignment with regional pole placement, J. Sound Vib. 494 (2021) 115858.
[29] R. Belotti, D. Richiedei, I. Tamellin, A. Trevisani, Pole assignment for active vibration control of linear vibrating systems through linear matrix inequalities, Appl. Sci. 10 (2020) 5494.
[30] D. Richiedei, I. Tamellin, Active approaches to vibration absorption through antiresonance assignment: A comparative study, Appl. Sci. 11 (2021) 1091.
[31] I. Bucher, S. Braun, The structural modification inverse problem: an exact solution, Mech. Syst. Signal Process. 7 (1993) 217–238.
[32] Z. Liu, W. Li, H. Ouyang, D. Wang, Eigenstructure assignment in vibrating systems based on receptances, Arch. Appl. Mech. 85 (2015) 713–724.
[33] S.-H. Tsai, H. Ouyang, J.-Y. Chang, Inverse structural modifications of a geared rotor-bearing system for frequency assignment using measured receptances, Mech. Syst. Signal Process. 110 (2018) 59–72.
[34] J. Hernandes, A. Suleman, Structural synthesis for prescribed target natural frequencies and mode shapes, Shock Vib. 2014 (2014).
[35] R. Belotti, D. Richiedei, A. Trevisani, Optimal design of vibrating systems through partial eigenstructure assignment, J. Mech. Des. 138 (2016) 071402.
[36] J. Mottershead, C. Mares, M. Friswell, An inverse method for the assignment of vibration nodes, Mech. Syst. Signal Process. 15 (2001) 87–100.
[37] R.A. Rojas, E. Wehrle, R. Vidoni, Optimal design for the passive control of vibration based on limit cycles, Shock Vib. 2019 (2019).
[38] R. Belotti, D. Richiedei, I. Tamellin, Antiresonance assignment in point and cross receptances for undamped vibrating systems, J. Mech. Des. 142 (2020).
[39] D. Richiedei, I. Tamellin, A. Trevisani, Simultaneous assignment of resonances and antiresonances in vibrating systems through inverse dynamic structural modification, J. Sound Vib. 485 (2020) 115552.
[40] C. Zang, M. Friswell, J. Mottershead, A review of robust optimal design and its application in dynamics, Comput. Struct. 83 (2005) 315–326.
[41] Z. Kang, S. Bai, On robust design optimization of truss structures with bounded uncertainties, Struct. Multidiscip. Optim. 47 (2013) 699–714.
[42] G. Spelsberg-Korspeter, Structural optimization for the avoidance of self-excited vibrations based on analytical models, J. Sound Vib. 329 (2010) 4829–4840.
[43] G. Spelsberg-Korspeter, Eigenvalue optimization against brake squeal: Symmetry, mathematical background and experiments, J. Sound Vib. 331 (2012) 4259–4268.
[44] T. Ritto, R. Lopez, R. Sampaio, J. Souza de Cursi, Robust optimization of a flexible rotor-bearing system using the campbell diagram, Eng. Optim. 43 (2011) 77–96.
[45] P. Gallina, M. Giovagnoni, Design of a screw jack mechanism to avoid self-excited vibrations, J. Dyn. Sys., Meas., Control. 124 (2002) 477–480.
[46] G.C. Marano, R. Greco, S. Sgobba, A comparison between different robust optimum design approaches: application to tuned mass dampers, Probab. Eng. Mech. 25 (2010) 108–118.
[47] S. Elias, V. Matsagar, Research developments in vibration control of structures using passive tuned mass dampers, Annu. Rev. Control 44 (2017) 129–156.
[48] N.C. Singer, W.P. Seering, Preshaping command inputs to reduce system vibration, J. Dyn. Syst. Meas. Control 112 (1990) 76–82.
[49] D. Richiedei, A. Trevisani, Shaper-based filters for the compensation of the load cell response in dynamic mass measurement, Mech. Syst. Signal Process. 98 (2018) 281–291.
[50] J. Vaughan, A. Yano, W. Singhose, Comparison of robust input shapers, J. Sound Vib. 315 (2008) 797–815.
[51] H. Ouyang, A hybrid control approach for pole assignment to second-order asymmetric systems, Mech. Syst. Signal Process. 25 (2011) 123–132.
[52] R. Belotti, D. Richiedei, A. Trevisani, Multi-domain optimization of the eigenstructure of controlled underactuated vibrating systems, Struct. Multidiscip. Optim. 63 (2021) 499–514.
[53] D. Richiedei, I. Tamellin, A. Trevisani, A homotopy transformation method for interval-based model updating of uncertain vibrating systems, Mech. Mach. Theory 160 (2021) 104288.
[54] I. Rivas-Cambero, J.M. Sausedo-Solorio, Dynamics of the shift in resonance frequency in a triple pendulum, Meccanica 47 (2012) 835–844.
[55] X. He, W. He, J. Shi, C. Sun, Boundary vibration control of variable length crane systems in two-dimensional space with output constraints, IEEE/ASME Trans. Mechatronics 22 (2017) 1952–1962.
[56] P. Merriaux, Y. Dupuis, R. Boutteau, P. Vasseur, X. Savatier, A study of vicon system positioning performance, Sensors 17 (2017) 1591.